Dominant role of symplectic symmetry in *ab initio* no-core shell model results for light nuclei

T. Dytrych, K. D. Sviratcheva, C. Bahri, and J. P. Draayer
Department of Physics and Astronomy, Louisiana State University, Baton Rouge, Louisiana 70803, USA

J. P. Vary
Department of Physics and Astronomy, Iowa State University, Ames, Iowa 50011, USA
(Received 9 April 2007; published 31 July 2007)

The symplectic Sp(3, $\mathbb{R}$) symmetry of eigenstates for the ^{16}O ground state and the 0^+_{gs} and lowest 2^+ and 4^+ configurations of ^{12}C that are determined within the framework of the no-core shell model with the JISP16 realistic interaction is examined. These states are found to project at the 80–85% level onto a few 0-particle-0-hole symplectic representations, including the most deformed configuration. The corresponding symplectic space spans 0-particle-0-hole nuclear configurations together with single- and multiparticle excitations. The results are nearly independent of the harmonic oscillator strength and whether the bare or renormalized effective interactions are used in the analysis. The outcome points to the relevance of a symplectic no-core shell model and reaffirms the Elliott SU(3) model on which the symplectic scheme is built.

DOI: 10.1103/PhysRevC.76.014315 PACS number(s): 21.60.Cs, 21.60.Fw, 21.10.Re, 27.20.+n

I. INTRODUCTION

The *ab initio* no-core shell model (NCSM) [1] has taken a prominent role in the development of microscopic tools for studying the structure of atomic nuclei. It has achieved a good description of the low-lying states in few-nucleon systems [2] as well as in more complex nuclei [1,3]. The NCSM incorporates intershell and core excitations within multishell spaces supported by complementary realistic interactions. Some recently developed realistic interactions that provide a reliable modeling of the essence of the strong interaction include J-matrix inverse scattering potentials [4], high-precision NN potentials derived from meson exchange theory [5], and nuclear two- and many-body forces based on chiral effective field theory [6].

It is the purpose of this work to present in more detail our findings [7] that low-lying states of the deformed ^{12}C and the "closed-shell" ^{16}O nuclei reflect the presence of an underlying symplectic $\mathfrak{sp}(3, \mathbb{R})$ algebraic structure.[1] This is achieved through the projection of realistic eigenstates determined in the framework of the NCSM with the JISP16 realistic interaction [4] onto Sp(3, $\mathbb{R}$)-symmetric basis states of the symplectic shell model that are free of spurious center-of-mass motion.

The symplectic shell model itself [8,9] is a microscopic realization of the successful Bohr-Mottelson collective model. It is also a multiple oscillator shell generalization of Elliott's SU(3) model. Symplectic algebraic approaches have achieved a very good reproduction of low-lying energies and $B(E2)$ values in light nuclei [10,11] and specifically in ^{12}C using phenomenological interactions [12] or truncated symplectic basis with simplistic (semi-) microscopic interactions [13,14]. Here, we establish, for the first time, the dominance of the symplectic Sp(3, $\mathbb{R}$) symmetry in nuclei as unveiled through *ab initio* calculations of the NCSM type with realistic interactions. This in turn provides a substantial insight into the physics and geometry of a nuclear system. Specifically, nuclear collective states with well-developed quadrupole and monopole vibrations as well as collective rotations are described naturally in terms of irreducible representations (irreps) of Sp(3, $\mathbb{R}$).

The outcome of the present study points to the possibility of achieving convergence of higher-lying collective modes and reaching heavier nuclei by a symplectic extension of the *ab initio* NCSM. The symplectic no-core shell model (Sp-NCSM) [7] amplifies on the NCSM concept by recognizing that deformed configurations often dominate and these, although typically described by only few collective Sp(3, $\mathbb{R}$) basis states, correspond to a special linear combination of a large number of NCSM basis states. Hence, for high-$\hbar\Omega$ collective modes the NCSM basis space can be extended beyond its current limits through Sp(3, $\mathbb{R}$) basis states. Thus the effective size of the model space can be significantly increased to include higher $\hbar\Omega$ values while constraining the growth in the size of the basis to a few symplectic symmetries that in the $0\hbar\Omega$ space reduce to SU(3) bandhead configurations. Although the present study focuses on the role of the 0-particle-0-hole (0p-0h) Sp(3, $\mathbb{R}$) irreps and symplectic excitations on top of these starting state configurations, highly deformed 2p-2h, 4p-4h, ..., np-nh Sp(3, $\mathbb{R}$) starting state configurations and symplectic excitations thereof can be readily included in the extended Sp-NCSM model space [7,15]. In this way, the Sp-NCSM with realistic interactions and with a multiple Sp(3, $\mathbb{R}$) irreps extension is expected to account for even higher $\hbar\Omega$ configurations required to realize experimentally measured $B(E2)$ values without an effective charge and to accommodate deformed spatial configurations [16] dictated by, for example, α-cluster modes in nuclei.

II. SYMPLECTIC Sp (3, $\mathbb{R}$) BASIS

The symplectic model [8,9] is based on the noncompact symplectic $\mathfrak{sp}(3, \mathbb{R})$ algebra. In its classical realization, the

[1] We use lowercase (capital) letters for algebras (groups).

symplectic symmetry underpins the dynamics of rotating bodies. For example, the Sp(3, $\mathbb{R}$) model has been used to describe the rotation of deformed stars and galaxies [17].

The significance of the symplectic symmetry for a microscopic description of a quantum many-body system of interacting particles [8,9] emerges from the physical relevance of its 21 generators. Specifically, the generators are constructed as bilinear products of the particle momentum ($p_{s\alpha}$) and coordinate ($q_{s\beta}$) operators such as $\sum_s p_{s\alpha} p_{s\beta}$, $\sum_s (q_{s\alpha} p_{s\beta} \pm q_{s\beta} p_{s\alpha})$, and $\sum_s q_{s\alpha} q_{s\beta}$ with $\alpha, \beta = x, y$, and z for the three spatial directions and s labeling an individual nucleon. The important observables, the many-particle kinetic energy $\sum_{s,\alpha} p_{s\alpha}^2/2m$, the mass quadrupole moment $\hat{Q}$, and angular momentum $\hat{L}$ operators are elements of the $\mathfrak{sp}(3, \mathbb{R}) \supset \mathfrak{su}(3) \supset \mathfrak{so}(3)$ algebraic structure. It also includes monopole and quadrupole collective vibrations reaching beyond a single shell to higher-lying and core configurations, as well as vorticity degrees of freedom for a description of rotational dynamics in a continuous range from irrotational to rigid rotor flows.

Alternatively, the elements of the $\mathfrak{sp}(3, \mathbb{R})$ algebra can be represented as bilinear products in harmonic oscillator (HO) raising ($b^\dagger$) and lowering (b) operators. In this realization, the natural set of the symplectic generators includes the HO Hamiltonian $\hat{H}_0$, which counts the total number of oscillator bosons, together with the eight single-shell SU(3) generators, $\hat{L}$ and $C^{(11)}_{\mathfrak{L}=2,M}$, as well as the six symplectic raising operators $A^{(20)}_{\mathfrak{L}M}$, which raise one particle by two shells, and their adjoints, the symplectic lowering operators $B^{(02)}_{\mathfrak{L}M}$. The many-particle kinetic energy is then given by, $\frac{1}{2}[H_0 - \sqrt{\frac{3}{2}}(A^{(20)}_{00} + B^{(02)}_{00})]$, and the mass quadrupole moment as $\hat{Q}_{2M} = \sqrt{3}(C^{(11)}_{2M} + A^{(20)}_{2M} + B^{(02)}_{2M})$.

The symplectic basis states are labeled (in standard notation [8,9]) according to the reduction chain

$$\begin{array}{ccccccc} \mathrm{Sp}(3,\mathbb{R}) & \supset & \mathrm{U}(3) & \supset & \mathrm{SU}(3) \\ \sigma & & n\rho & \omega & \kappa & L \end{array} \tag{1}$$

and are constructed by acting with polynomials $\mathcal{P}$ in the symplectic raising operator, $A^{(20)}$, on a set of basis states of the symplectic bandhead, $|\sigma\rangle$, which is a Sp(3, $\mathbb{R}$) lowest-weight state ($B^{(02)}|\sigma\rangle = 0$); that is,

$$|\sigma n \rho \omega \kappa (LS) J M_J\rangle = [\mathcal{P}^n(A^{(20)}) \times |\sigma\rangle]^{\rho\omega}_{\kappa(LS)JM_J}, \tag{2}$$

where $\sigma \equiv N_\sigma(\lambda_\sigma \mu_\sigma)$ labels Sp(3, $\mathbb{R}$) irreps with $(\lambda_\sigma \mu_\sigma)$ denoting a SU(3) lowest-weight state, $n \equiv N_n(\lambda_n \mu_n)$, and $\omega \equiv N_\omega(\lambda_\omega \mu_\omega)$. The quantum number $N_\omega = N_\sigma + N_n$ is the total number of oscillator quanta related to the eigenvalue, $N_\omega \hbar\Omega$, of a HO Hamiltonian that is free of spurious modes. The $(\lambda_n \mu_n)$ set gives the overall SU(3) symmetry of $\frac{N_n}{2}$ coupled raising operators in $\mathcal{P}$ and $(\lambda_\omega \mu_\omega)$ specifies the SU(3) symmetry of the symplectic state. Consequently, the symplectic basis states bring forward important information about the nuclear shapes and deformation in terms of the SU(3) labels, $(\lambda_\omega \mu_\omega)$, for example, (00), ($\lambda$0) and (0$\mu$) describe spherical, prolate and oblate shapes, respectively.

The symplectic raising operator $A^{(20)}_{\mathfrak{L}M}$, $\mathfrak{L} = 0, 2$, is a SU(3) tensor with $(\lambda\mu) = (20)$ character,

$$A^{(20)}_{\mathfrak{L}M} = \frac{1}{\sqrt{2}} \sum_i [b_i^\dagger \times b_i^\dagger]^{(20)}_{\mathfrak{L}M} - \frac{1}{\sqrt{2}A} \sum_{s,t} [b_s^\dagger \times b_t^\dagger]^{(20)}_{\mathfrak{L}M}, \tag{3}$$

where the sums are over all A particles of the system. The first term raises one particle by two shells, that is it induces $2\hbar\Omega$ one-particle-one-hole (1p-1h) monopole ($\mathfrak{L} = 0$) or quadrupole ($\mathfrak{L} = 2$) excitations. The second term is included to eliminate the spurious center-of-mass excitations in the symplectic states (2) and introduces $2\hbar\Omega$ 2p-2h configurations (two particles raised by one shell each). Both one and two body matrix elements of the symplectic raising operator in a three-dimensional HO (m-scheme) basis, which is the same basis used in the NCSM, are given in Appendix A.

A symplectic state of a HO excitation energy N_ω (2) can be constructed by the action of the symplectic raising operator $A^{(20)}$ on a linear combination of symplectic states of $N'_\omega = N_\omega - 2$ excitation energy,

$$\begin{aligned} |\sigma n \rho \omega \kappa (LS) J M_j\rangle &= (-1)^S \sqrt{2L+1} \sum_{\mathfrak{L}M} A^{(20)}_{\mathfrak{L}M} \\ &\times \sum_{n'\rho'\omega'} U[(20)(\lambda'_n \mu'_n)(\lambda_\omega \mu_\omega)(\lambda_\sigma \mu_\sigma); (\lambda_n \mu_n) 1 \rho(\lambda'_\omega \mu'_\omega) \rho' 1] \\ &\times \sum_{\kappa' L'} \langle (20)\mathfrak{L}; (\lambda'_\omega \mu'_\omega) \kappa' L' \| (\lambda_\omega \mu_\omega) \kappa L \rangle \\ &\times \sum_{J'M'_j} (-1)^{J'+L'} \sqrt{2J'+1} \begin{Bmatrix} L' & S & J' \\ J & \mathfrak{L} & L \end{Bmatrix} \\ &\times C^{JM_j}_{J'M'_j \mathfrak{L}M} \delta_{N'_n, N_n - 2} \delta_{N'_\omega, N_\omega - 2} |\sigma n' \rho' \omega' \kappa' (L'S) J' M'_j\rangle, \end{aligned} \tag{4}$$

where $U[(20)(\lambda'_n \mu'_n)(\lambda_\omega \mu_\omega)(\lambda_\sigma \mu_\sigma); (\lambda_n \mu_n) 1 \rho(\lambda'_\omega \mu'_\omega) \rho' 1]$ is a SU(3)-Racah coefficient, $C^{JM_j}_{J'M'_j \mathfrak{L}M}$ and $\langle (20)\mathfrak{L}; (\lambda'_\omega \mu'_\omega) \kappa' L' \| (\lambda_\omega \mu_\omega) \kappa L \rangle$ denote SU(2) and reduced SU(3) $\supset$ SO(3) Clebsch-Gordan coefficients, respectively, and $\{ \begin{smallmatrix} L' & S & J' \\ J & \mathfrak{L} & L \end{smallmatrix} \}$ is a Wigner 6j coefficient. This formula greatly facilitates the process of generating the symplectic basis as it makes use of the symplectic states of lower excitation energies that are computed only once. It also makes parallel implementation of the basis construction formula (2) rather straightforward.

The base case for the formula (4) is the m-scheme realization of the basis states $|\sigma \kappa (L_0 S_0) J_0 M_0\rangle$ of the symplectic bandhead, $|\sigma\rangle$, for $n = 0(00)$, $\rho = 1$, and $\omega = \sigma$. The symplectic bandhead basis states are constructed as SU(3)-symmetric linear combinations of all possible fermion configurations of a given N_σ, that for 0p-0h corresponds to the lowest HO energy of a system of A nucleons; that is,

$$\begin{aligned} &|(\gamma) \sigma \kappa (L_0 S_0) J_0 M_0\rangle \\ &\quad = \left[\mathcal{P}^{(\lambda_\pi \mu_\pi)}_{S_\pi}(a^\dagger_\pi) \times \mathcal{P}^{(\lambda_\nu \mu_\nu)}_{S_\nu}(a^\dagger_\nu) \right]^{(\lambda_\sigma \mu_\sigma)}_{\kappa(L_0 S_0) J_0 M_0} |0\rangle, \end{aligned} \tag{5}$$

where $|0\rangle$ is a vacuum state, the additional quantum number γ is included to distinguish between different bandhead constructions for protons and neutrons $\{(\lambda_\pi \mu_\pi) S_\pi, (\lambda_\nu \mu_\nu) S_\nu\}$,

and $\mathcal{P}^{(\lambda_\pi \mu_\pi)}_{S_\pi}$ and $\mathcal{P}^{(\lambda_\nu \mu_\nu)}_{S_\nu}$ denote polynomials of proton ($a^\dagger_\pi$) and neutron ($a^\dagger_\nu$) creation operators coupled to good SU(3) × SU(2) symmetry. This is done by recognizing that the fermion creation operators are SU(3) × SU(2) tensors $a^\dagger_{\eta(l\frac{1}{2})jm_j} \to a^\dagger_{(\eta 0)(l\frac{1}{2})jm_j}$ with a SU(3) character of $(\eta 0)$, where $\eta = 0, 1, 2, \ldots$ labels a HO shell and $l = \eta, \eta - 2, \ldots, 0(1)$. The construction described above is performed in a proton-neutron formalism. Hence, the symplectic states used in our analysis do not have good isospin.

III. RESULTS AND DISCUSSIONS

A. Ground-state rotational band in the ^{12}C nucleus: wave functions and $B(E2 : 2^+_1 \to 0^+_{gs})$ transition rates

The lowest-lying eigenstates of ^{12}C were calculated using the NCSM as implemented through the many fermion dynamics (MFD) code [18] with an effective interaction derived from the realistic JISP16 NN potential [4] for different $\hbar\Omega$ oscillator strengths. (The JISP16 interaction is a pure two-body interaction that provides for rapid convergence in NCSM applications, and although it does not contain three-body (NNN) terms, it yields results that are comparable with shell model calculations that use realistic NN+NNN potentials. This is achieved through off-shell variations of JISP16 which are fitted to properties of $A = 3$, 6 and 16 nuclei in order to accommodate significant NN interaction contributions.) We are particularly interested in the $J = 0^+_{gs}$ and the lowest $J = 2^+ (\equiv 2^+_1)$ and $J = 4^+ (\equiv 4^+_1)$ states of the ground-state (gs) rotational band, which appear to be reasonably converged in the $N_{max} = 6$ NCSM basis space. In addition, calculated binding energies and other observables, such as ground-state proton rms radii and the 2^+_1 quadrupole moment, all lie reasonably close to the measured values. The electromagnetic transition strengths, $B(E2; 2^+_1 0 \to 0^+_{gs} 0)$, $B(E2; 2^+_1 1 \to 0^+_{gs} 0)$ and $B(M1; 1^+_1 1 \to 0^+_{gs} 0)$, are still underestimated, yielding just over 60% of the corresponding experimental strengths. Additional contributions are expected to arise from higher basis states producing more complete formation of the exponential tails of the wave functions to which these observables are sensitive.

For ^{12}C there are 13 distinct 0p-0h Sp(3, $\mathbb{R}$) irreps (Table I), which are built over the symplectic bandhead basis states, $|\sigma\rangle$, with $N_\sigma = 24.5$. For each 0p-0h Sp(3, $\mathbb{R}$) irrep we generated basis states according to (2) up to $N_{max} = 6$ ($6\hbar\Omega$ model space). Analysis of overlaps of the symplectic states with the NCSM eigenstates for the 0^+_{gs} and the lowest 2^+ and 4^+ states reveals non-negligible overlaps for only 3 of the 13 0p-0h Sp(3, $\mathbb{R}$) ($N_\sigma = 24.5$) irreps, specifically, the leading (most deformed) representation $(\lambda_\sigma \mu_\sigma) = (04)$ carrying spin $S = 0$ together with the two $S = 1(1\,2)$ irreps in Table I. Had we adopted the supermultiplet formalism, we would have obtained two $S = 1(1\,2)$ irreps, one with isospin $T = 0$ and the other with $T = 1$. In this case, only one of the two $S = 1(1\,2)$ irreps is expected to significantly contribute (T = 0), whereas the other state of definite isospin may only slightly mix because of the presence of the Coulomb interaction.

TABLE I. 0p-0h Sp(3, $\mathbb{R}$) irreps in ^{12}C, $N_\sigma = 24.5$.

$(\lambda_\pi \mu_\pi) S_\pi$	$\otimes$	$(\lambda_\nu \mu_\nu) S_\nu$	$\to$	$(\lambda_\sigma \mu_\sigma)$	S
$(02) S_\pi = 0$		$(02) S_\nu = 0$		(04)(12) (20)	S = 0
$(02) S_\pi = 0$		$(10) S_\nu = 1$		(01)(12)	S = 1
$(10) S_\pi = 1$		$(02) S_\nu = 0$		(01)(12)	S = 1
$(10) S_\pi = 1$		$(10) S_\nu = 1$		(01)(20)	S = 0, 1, 2

The overlaps of the most dominant symplectic states with the NCSM eigenstates for the 0^+_{gs}, 2^+_1, and 4^+_1 states in the 0, 2, 4, and $6\hbar\Omega$ subspaces are given for $\hbar\Omega = 12$ MeV (Table II) and $\hbar\Omega = 15$ MeV (Table III). To speed up the calculations, we retained only the largest amplitudes of the NCSM states, those sufficient to account for at least 98% of the norm, which is quoted also in the tables. The results show that typically more than 80% of the NCSM eigenstates fall within a subspace spanned by the 3 leading 0p-0h Sp(3, $\mathbb{R}$) irreps. The most deformed irrep $(04)S = 0$ is clearly dominant, its overlap with all three NCSM eigenstates ranges from about 65% to just under 75% with the $\hbar\Omega = 12$ MeV results about 5% higher than those for $\hbar\Omega = 15$ MeV. This reveals the significance of the $(04)S = 0$ irrep, which in the framework of the symplectic shell model gives rise to a prominent $J = 0$, 2, and 4 rotational structure and hence it is suitable for a microscopic description of the ground-state rotational band in ^{12}C [12]. The outcome also demonstrates that the dominance of the three symplectic irreps is consistent throughout the band. The mixing of the two $(12)S = 1$ irreps is comparatively much smaller for all the three 0^+_{gs}, 2^+_1, and 4^+_1 states, yet it may affect electric quadrupole transitions from higher-lying $J = 0$, 2, and 4 states toward the ground-state band.

Examination of the role of the model space truncation specified by $N_{max}\hbar\Omega$ reveals that the general features of all outcomes are retained as the space is expanded from $2\hbar\Omega$ to $6\hbar\Omega$ (see, e.g., Fig. 1 for 0^+_{gs}). This includes the dominance of the most deformed $(0\,4)S = 0$ irrep as well as the $0\hbar\Omega$ configurations. In addition, the same three Sp(3, $\mathbb{R}$) irreps dominate for all N_{max} values with the large overlaps of the NCSM eigenstates with the leading symplectic irreps preserved, albeit distributed outward across higher $\hbar\Omega$ excitations as the number of active shells increases. In this regard, it may be interesting to

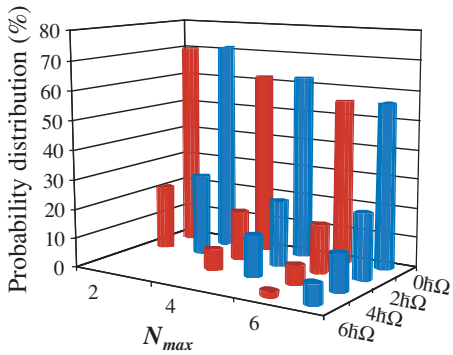

FIG. 1. (Color online) NCSM (blue, right) and 0p-0h Sp(3, $\mathbb{R}$) (red, left) probability distribution over $0\hbar\Omega$ to $N_{max}\hbar\Omega$ subspaces for the 0^+_{gs} of ^{12}C for different model spaces, N_{max}, with $\hbar\Omega = 15$ MeV.

TABLE II. Probability distribution of NCSM eigenstates for ^{12}C across the leading 3 0p-0h Sp(3, $\mathbb{R}$) irreps, $\hbar\Omega = 12$ MeV.

		$0\hbar\Omega$	$2\hbar\Omega$	$4\hbar\Omega$	$6\hbar\Omega$	Total
			$J = 0$			
	$(0\,4)S = 0$	41.39	19.66	8.73	3.14	72.92
Sp(3, $\mathbb{R}$)	$(1\,2)S = 1$	2.24	1.49	0.80	0.41	4.94
	$(1\,2)S = 1$	2.19	1.46	0.78	0.41	4.84
	Total	45.82	22.61	10.31	3.96	82.70
NCSM		45.90	27.41	15.89	9.03	98.23
			$J = 2$			
	$(0\,4)S = 0$	41.20	19.34	8.44	3.06	72.04
Sp(3, $\mathbb{R}$)	$(1\,2)S = 1$	2.50	1.51	0.77	0.38	5.16
	$(1\,2)S = 1$	2.42	1.47	0.75	0.37	5.01
	Total	46.12	22.32	9.96	3.81	82.21
NCSM		46.19	27.10	15.76	9.25	98.30
			$J = 4$			
	$(0\,4)S = 0$	44.21	19.23	8.01	2.91	74.36
Sp(3, $\mathbb{R}$)	$(1\,2)S = 1$	1.69	0.90	0.44	0.21	3.24
	$(1\,2)S = 1$	1.68	0.89	0.43	0.21	3.21
	Total	47.58	21.02	8.88	3.33	80.81
NCSM		47.59	25.87	15.24	9.46	98.16

understand the importance of the latter beyond the $6\hbar\Omega$ model space and their role in shaping other low-lying states in ^{12}C such as the second 0^+, which is likely to reflect a clusterlike behavior (e.g., see Ref. [19]). This task, albeit challenging, is feasible for the no-core shell model with symplectic Sp(3, $\mathbb{R}$) extension and will be part of a follow-on study.

The 0^+_{gs} and 2^+_1 states, constructed in terms of the three Sp(3, $\mathbb{R}$) irreps with probability amplitudes defined by the overlaps with the ^{12}C NCSM wave functions, were also used to determine $B(E2)$ transition rates. These quantities, compared to the energy of the lowest-lying states in light nuclei, are typically less accurately reproduced by present-day models with realistic interactions. The Sp(3, $\mathbb{R}$)$B(E2 : 2^+_1 \to 0^+_{gs})$ values clearly reproduce the NCSM results, namely they slightly increase from 101% to 107% of the corresponding NCSM numbers with increasing $\hbar\Omega$ (Fig. 2). In addition, if only the leading most deformed (0 4) Sp(3, $\mathbb{R}$) irrep is considered, that is without the mixing due to both (1 2)$S = 1$ irreps, the $B(E2 : 2^+_1 \to 0^+_{gs})$ values increase only by 5–12%. In this regard, the leading (0 4) Sp(3, $\mathbb{R}$) irrep, in addition

TABLE III. Probability distribution of NCSM eigenstates for ^{12}C across the leading 3 0p-0h Sp(3, $\mathbb{R}$) irreps, $\hbar\Omega = 15$ MeV.

		$0\hbar\Omega$	$2\hbar\Omega$	$4\hbar\Omega$	$6\hbar\Omega$	Total
			$J = 0$			
	$(0\,4)S = 0$	46.26	12.58	4.76	1.24	64.84
Sp(3, $\mathbb{R}$)	$(1\,2)S = 1$	4.80	2.02	0.92	0.38	8.12
	$(1\,2)S = 1$	4.72	1.99	0.91	0.37	7.99
	Total	55.78	16.59	6.59	1.99	80.95
NCSM		56.18	22.40	12.81	7.00	98.38
			$J = 2$			
	$(0\,4)S = 0$	46.80	12.41	4.55	1.19	64.95
Sp(3, $\mathbb{R}$)	$(1\,2)S = 1$	4.84	1.77	0.78	0.30	7.69
	$(1\,2)S = 1$	4.69	1.72	0.76	0.30	7.47
	Total	56.33	15.90	6.09	1.79	80.11
NCSM		56.63	21.79	12.73	7.28	98.43
			$J = 4$			
	$(0\,4)S = 0$	51.45	12.11	4.18	1.04	68.78
Sp(3, $\mathbb{R}$)	$(1\,2)S = 1$	3.04	0.95	0.40	0.15	4.54
	$(1\,2)S = 1$	3.01	0.94	0.39	0.15	4.49
	Total	57.50	14.00	4.97	1.34	77.81
NCSM		57.64	20.34	12.59	7.66	98.23

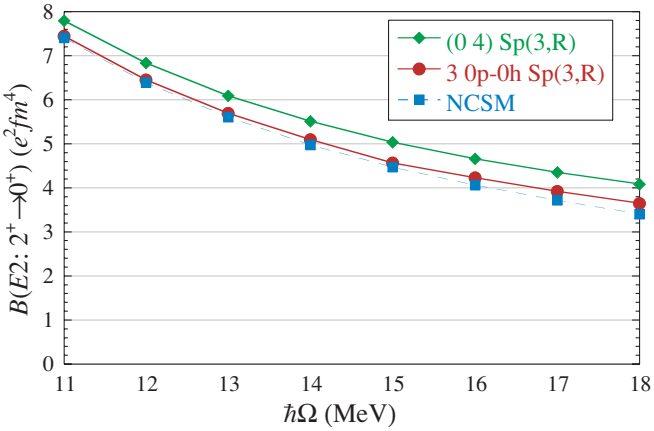

FIG. 2. (Color online) NCSM and Sp(3, $\mathbb{R}$)$B(E2 : 2_1^+ \rightarrow 0_{gs}^+)$ transition rate in e^2 fm^4 for ^{12}C as a function of the $\hbar\Omega$ oscillator strength in MeV, $N_{max} = 6$.

to its large projection onto the realistic eigenstates, suffices to achieve a quite good reproduction of the NCSM $B(E2)$ estimate.

B. Ground state in the ^{16}O nucleus

The proper microscopic description of the low-lying states of ^{16}O has been a long-standing challenge for the shell model studies [20–25]. The ground state of ^{16}O, which is reasonably well converged in NCSM calculations, is included in our analysis. In the case of ^{16}O there is only one possible 0p-0h Sp(3, $\mathbb{R}$) irrep, namely, $N_\sigma = 34.5(\lambda_\sigma \mu_\sigma) = (00)$ and spin $S = 0$, with a symplectic bandhead coinciding with the single $0\hbar\Omega$ NCSM Slater determinant. As in the ^{12}C case, for the 0p-0h Sp(3, $\mathbb{R}$) irrep we generated basis states according to (2) up to $N_{max} = 6$ ($6\hbar\Omega$ model space). These are compared to the results of the NCSM with the bare and effective realistic JISP16 interaction [4] as implemented through the many fermion dynamics (MFD) code [18].

Consistent with the outcome for ^{12}C, the projection of the NCSM eigenstates onto the symplectic basis reveals a large Sp(3, $\mathbb{R}$)-symmetric content in the ground-state wave function (Tables IV and V). Here again, we retained only the largest amplitudes of the NCSM states, those sufficient to account for at least 98% of the norm. The results show that 75–80% of the NCSM eigenstate for ^{16}O fall within a subspace spanned by the single irrep (00) for ^{16}O.

In short, the low-lying states under consideration are well described in terms of only three 0p-0h Sp(3, $\mathbb{R}$) irreps for ^{12}C and only one 0p-0h Sp(3, $\mathbb{R}$) irrep for ^{16}O, revealing a clear dominance of the leading collective configuration, the most deformed $(04)S = 0$ in ^{12}C and $(00)S = 0$ in ^{16}O.

TABLE IV. Probability distribution of the NCSM eigenstate for the $J = 0$ ground state in ^{16}O across the 0p-0h Sp(3, $\mathbb{R}$) irrep, $\hbar\Omega =$ 12 MeV.

	$0\hbar\Omega$	$2\hbar\Omega$	$4\hbar\Omega$	$6\hbar\Omega$	Total
Sp(3, $\mathbb{R}$) $(00)S = 0$	38.73	23.92	11.89	5.28	79.82
NCSM	38.73	28.78	18.80	12.66	98.97

TABLE V. Probability distribution of the NCSM eigenstate for the $J = 0$ ground state in ^{16}O across the 0p-0h Sp(3, $\mathbb{R}$) irrep, $\hbar\Omega =$ 15 MeV.

	$0\hbar\Omega$	$2\hbar\Omega$	$4\hbar\Omega$	$6\hbar\Omega$	Total
Sp(3, $\mathbb{R}$) $(00)S = 0$	50.53	15.87	6.32	2.30	75.02
NCSM	50.53	22.58	14.91	10.81	98.83

C. Large reduction of model space dimension

The typical dimension of a symplectic irrep basis in the $N_{max} = 6$ space is on the order of 10^2 as compared to 10^7 for the full NCSM m-scheme basis space. Moreover, the space spanned by a given symplectic irrep, σ, can be decomposed to subspaces of a definite J angular momentum (see Eq. (2)) and can be further reduced to only the subspaces specified by the J values under consideration. In the case of ^{12}C, these are $J = 0, 2$, and 4, and for ^{16}O it is $J = 0$. As the model space, N_{max}, is increased the dimension of the $J = 0, 2$, and 4 symplectic space built on the 13 0p-0h Sp(3, $\mathbb{R}$) irreps grows very slowly compared to the NCSM space dimension (Table VI). The dominance of only three irreps additionally reduces the dimensionality of the symplectic model space (Table VI), which in the $12\hbar\Omega$ model space constitutes only 3.7×10^{-6}% of the NCSM space size. The space reduction is even more dramatic in the case of ^{16}O (Table VI, last two rows). This means that a space spanned by a set of symplectic basis states may be computationally manageable even when high-$\hbar\Omega$ configurations are included. It is important to note that $2\hbar\Omega$ 2p-2h (two particles raised by one shell each) and higher rank np-nh excitations and allowed multiples thereof can be included by building them into an expanded set of lowest-weight Sp(3, $\mathbb{R}$) starting state configurations. The same "build-up" logic, (2), holds because by construction these additional starting state configurations are also required to be lowest-weight Sp(3, $\mathbb{R}$) states. Note that if one were to include all possible lowest-weight np-nh starting state configurations ($n \leqslant N_{max}$), and allowed multiples thereof, one would span the entire NCSM space.

In short, the symplectic subspace for the low-lying states in ^{12}C and ^{16}O that achieves large overlaps with the realistic NCSM eigenstates and reproduction of the NCSM estimates for the $B(E2)$ transition rates comprises only a small fraction of the full NCSM model space.

D. Symplectic invariance within the spin parts of realistic eigenstates

Another striking property of the low-lying eigenstates is revealed when the spin projections of the converged NCSM states are examined. Specifically, the $S = 0$ symplectic irrep, (0 4), accounts for around 90% of the corresponding $S = 0$ part of the NCSM realistic eigenstates for the 0_{gs}^+, 2_1^+ and 4_1^+ in ^{12}C that are calculated in a $6\hbar\Omega$ model space (Fig. 3). The

TABLE VI. Model spaces dimension for different maximum allowed $\hbar\Omega$ excitations, $N_{\max}$, for the NCSM and the 3 most significant 0p-0h Sp(3, $\mathbb{R}$) irreps limited to $J = 0$, 2, and 4 states in ^{12}C and the only one 0p-0h Sp(3, $\mathbb{R}$) irrep limited to $J = 0$ in ^{16}O. For comparison, the size of the full space of the 3 0p-0h Sp(3, $\mathbb{R}$) irreps (all J values) is shown together with the $J = 0$, 2, and 4 model space dimension of all the 13 0p-0h Sp(3, $\mathbb{R}$) irreps for ^{12}C.

	$N_{\max}$						
	$0\hbar\Omega$	$2\hbar\Omega$	$4\hbar\Omega$	$6\hbar\Omega$	$8\hbar\Omega$	$10\hbar\Omega$	$12\hbar\Omega$
			^{12}C				
NCSM	51	1.77×10^4	1.12×10^6	3.26×10^7	5.94×10^8	7.83×10^9	8.08×10^{10}
3 Sp(3, $\mathbb{R}$) irreps, $J = 0, 2, 4$	13	68	216	514	1030	1828	2979
3 Sp(3, $\mathbb{R}$) irreps, all J	21	127	444	1098	2414	4674	8388
13 Sp(3, $\mathbb{R}$) irreps $J = 0, 2, 4$	30	157	495	1169	2326	4103	6651
			^{16}O				
NCSM	1	1.24×10^3	3.44×10^5	2.61×10^7	9.70×10^8	2.27×10^{10}	3.83×10^{11}
1 Sp(3, $\mathbb{R}$) irrep, $J = 0$	1	2	4	7	11	16	23

results are independent of the $\hbar\Omega$ oscillator strength as well as if the bare interaction is used. As for the $S = 1$ part, the overlap with the two $S = 1(1\,2)$ symplectic irreps is around 80% for the 0^+_{gs} and 2^+_1 and around 70% for 4^+_1. The results further reveal that, for example, for the 0^+_{gs} state, within each $\hbar\Omega$ subspace on average only 1–1.5% of the NCSM 0^+_{gs} are not accounted for by the $S = 0$ ($S = 1$) Sp(3, $\mathbb{R}$) irrep(s) under consideration. In summary, the $S = 0$ plus $S = 1$ part of the NCSM wave function is very well explained by only the three Sp(3, $\mathbb{R}$) collective configurations.

In the case of ^{16}O, the leading $S = 0$ symplectic irrep, (00), projects at the 90% level onto the $S = 0$ component of the 0^+_{gs} eigenstate for all values of $\hbar\Omega$ and for the bare interaction (Fig. 3).

Clearly, as shown in Fig. 3, the Sp(3, $\mathbb{R}$) symmetry of the low-lying eigenstates and hence the geometry of the nuclear system is described as nearly independent of the $\hbar\Omega$ oscillator strength. The symplectic symmetry is present with equal strength in the spin parts of the NCSM wave functions for ^{12}C as well as ^{16}O regardless of whether the bare or the effective interactions are used. This suggests that the transformation to an effective interaction, which compensates for the finite space truncation by renormalization of the bare interaction, does not affect the Sp(3, $\mathbb{R}$) symmetry structure of the spatial wave functions. Hence, the symplectic structure detected in the present analysis for $6\hbar\Omega$ model space is what would emerge in NSCM evaluations with a sufficiently large model space to justify use of the bare interaction.

Although the spatial symmetry within a spin component is nearly constant, the renormalization of the bare interaction and $\hbar\Omega$ variations influence the spin content of the eigenstates. Comparatively strong spin mixing is related to spin-orbit effects. For example, in ^{12}C the $S = 0$ ($S = 1$) part of the NCSM eigenstates under consideration decrease (increase) toward higher $\hbar\Omega$ frequencies (Fig. 4). This is the reason why the projection of the NCSM wave functions onto the

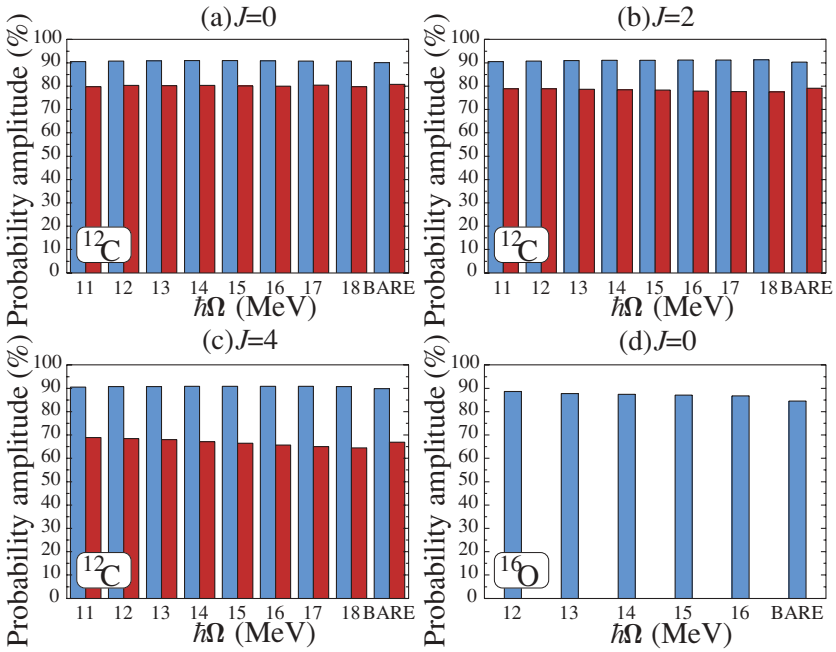

FIG. 3. (Color online) Projection of the $S = 0$ (blue, left) (and $S = 1$ (red, right)) 0p-0h Sp(3, $\mathbb{R}$) irreps onto the corresponding significant spin components of the NSCM wave functions for (a) 0^+_{gs}, (b) 2^+_1, and (c) 4^+_1 in ^{12}C and (d) 0^+_{gs} in ^{16}O, for effective interaction for different $\hbar\Omega$ oscillator strengths and bare interaction. (We present only the most significant spin values that account for around 90% of a NCSM wave function.)

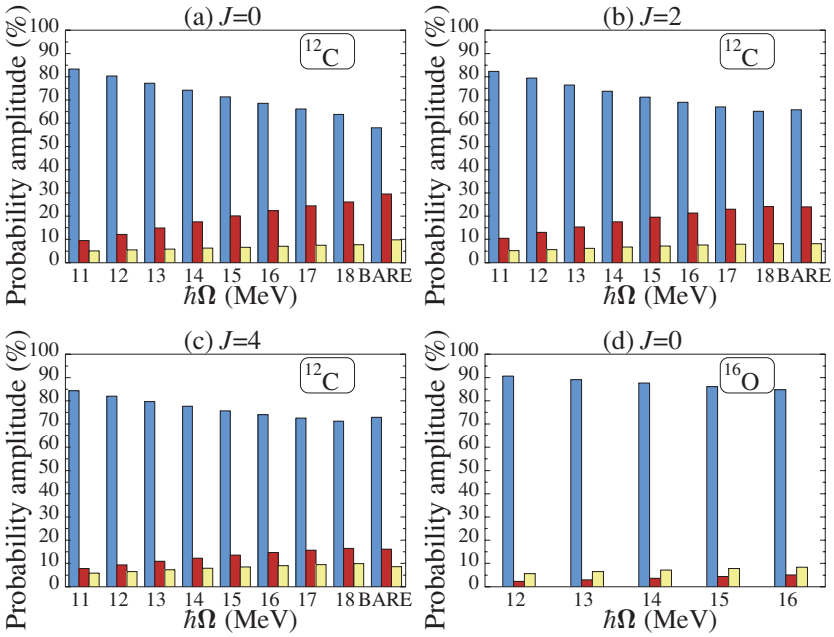

FIG. 4. (Color online) Probability amplitudes for the $S = 0$ (blue, left), $S = 1$ (red, middle), and $S = 2$ (yellow, right) components of the NCSM eigenstates for (a) 0^+_{gs}, (b) 2^+_1, and (c) 4^+_1 in ^{12}C and (d) 0^+_{gs} in ^{16}O, $N_{max} = 6$.

symplectic space slightly changes as one varies the oscillator strength $\hbar\Omega$ (Fig. 5 and Tables II and III). The symplectic structure is preserved, specifically the 3 Sp(3, $\mathbb{R}$) irreps, (0 4)$S = 0$ and the two (1 2)$S = 1$, remain dominant, only the Sp(3, $\mathbb{R}$) irrep contributions change reflecting the spin redistribution. Likewise, for the ^{16}O case the overlap of the leading (0 0)$S = 0$ Sp(3, $\mathbb{R}$) irrep with the realistic eigenstate follows the decrease, toward large $\hbar\Omega$ values, of the probability amplitude of the $S = 0$ component in the NCSM wave function (Fig. 5(d)).

As one varies the oscillator strength $\hbar\Omega$ (Fig. 5), the overall overlaps increase toward smaller $\hbar\Omega$ HO frequencies and, for example, for the 0^+_{gs} it is 85% for ^{12}C and 80% for ^{16}O in the $N_{max} = 6$ and $\hbar\Omega = 11$ MeV case. As expected, Fig. 5 also confirms that with increasing $\hbar\Omega$ the high $\hbar\Omega$ excitations contribute less as the lower-lying shell configurations become energetically more favorable.

Although the focus here has been on demonstrating the existence of Sp(3, $\mathbb{R}$) symmetry in NCSM results for ^{12}C and ^{16}O, and therefore a possible path forward for extending the NCSM to a Sp-NCSM scheme, the results can also be interpreted as a further strong confirmation of Elliott's SU(3) model because the projection of the NCSM states onto the $0\hbar\Omega$ space [Fig. 5, blue (right) bars] is a projection of the NCSM results onto the SU(3) shell model. For example, for ^{12}C the $0\hbar\Omega$ SU(3) symmetry ranges from just over 40% of the NCSM 0^+_{gs} for $\hbar\Omega = 11$ MeV to nearly 65% for $\hbar\Omega = 18$ MeV [Fig. 5, blue (left) bars] with 80–90% of this symmetry

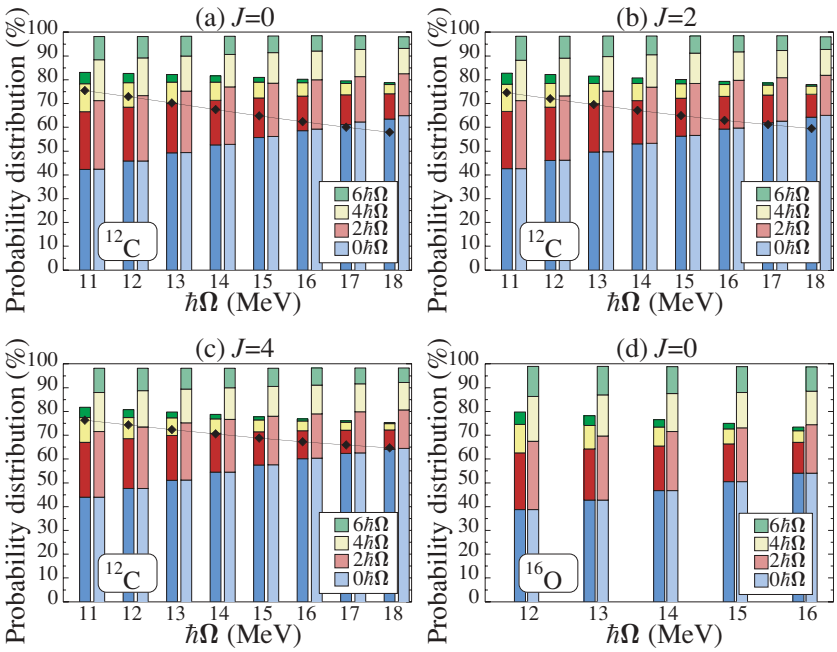

FIG. 5. (Color online) Probability distribution for the (a) 0^+_{gs}, (b) 2^+_1, and (c) 4^+_1 states in ^{12}C and (d) 0^+_{gs} in ^{16}O over $0\hbar\Omega$ (blue, lowest) to $6\hbar\Omega$ (green, highest) subspaces for the 3 0p-0h Sp(3, $\mathbb{R}$) irrep case (left) and NCSM (right) together with the (0 4) irrep contribution (black diamonds) in ^{12}C as a function of the $\hbar\Omega$ oscillator strength in MeV for $N_{max} = 6$.

governed by the leading (04) irrep. These numbers are consistent with what has been shown to be a dominance of the leading SU(3) symmetry for SU(3)-based shell-model studies with realistic interactions in $0\hbar\Omega$ model spaces. It seems the simplest of Elliott's collective states can be regarded as a good first-order approximation in the presence of realistic interactions, whether the latter is restricted to a $0\hbar\Omega$ model space or the richer multi-$\hbar\Omega$ NCSM model spaces.

IV. CONCLUSION

We have demonstrated that *ab initio* NCSM analysis starting with the JISP16 nucleon-nucleon interaction displays a clear symplectic symmetry structure, which moreover remains unaltered whether the bare or effective interactions for various $\hbar\Omega$ strengths are used. As a "proof-of-principle" our study focuses on the lowest $0^+_{\rm gs}$, 2^+_1, and 4^+_1 states in the deformed ^{12}C nucleus and the $0^+_{\rm gs}$ ground state in the "closed-shell" ^{16}O nucleus. The analysis of the results reveals that the NCSM eigenstates project at approximately the 80% level onto only a few 0p-0h spurious center-of-mass free symplectic irreps with a clear dominance of the leading Sp(3, $\mathbb{R}$) irrep. Furthermore, in the case of the ^{12}C ground-state rotational band the three most significant 0p-0h Sp(3, $\mathbb{R}$) irreps yield a $B(E2: 2^+_1 \to 0^+_{\rm gs})$ transition rate that almost exactly agrees with the NCSM $B(E2)$ estimates. The close reproduction of the NCSM results is achieved by a Sp(3, $\mathbb{R}$)-symmetric subspace with a dimensionality only $\approx 10^{-3}\%$ that of the full NCSM space.

The results confirm for the first time the validity of the Sp(3, $\mathbb{R}$) approach when realistic interactions are invoked. This demonstrates the importance of the Sp(3, $\mathbb{R}$) symmetry, which simply matches the nuclear geometry to the many-nucleon dynamics, as well as reaffirms the value of the simpler SU(3) model on which it is based.

The results further suggest that a Sp-NCSM extension of the NCSM may be a practical scheme for achieving convergence to measured $B(E2)$ values without the need for introducing an effective charge and even for modeling cluster-like phenomena as these modes can be accommodated within the general framework of the Sp(3, $\mathbb{R}$) model [16] if extended to large model spaces (high $N_{\rm max}$). In addition, the Sp-NCSM scheme, which is "structured" to take advantage of massively parallel computing capability, holds promise to allow us to model heavier nuclei, including neutron-deficient and $N \approx Z$ nuclei, along the nucleosynthesis rp path and unstable nuclei currently explored in radioactive beam experiments.

In short, the NCSM with a modern realistic NN potential supports the development of collective motion in nuclei as can be realized within the framework of the Sp-NCSM and as is apparent in its $0\hbar\Omega$ Elliott model limit.

ACKNOWLEDGMENTS

This work was supported by the U.S. National Science Foundation, Grants 0140300 and 0500291, and the Southeastern Universities Research Association, as well as, in part, by the U.S. Department of Energy Grant DE-FG02-87ER40371. Tomáš Dytrych acknowledges supplemental support from the Graduate School of Louisiana State University. Further, discussions with many colleagues, but especially Bruce R. Barrett, during the initial phases of this project are gratefully acknowledged.

APPENDIX A: MATRIX ELEMENTS OF THE SYMPLECTIC RAISING OPERATOR $A^{(20)}_{\mathfrak{L}M}$

Matrix elements of the one body part of the $A^{(20)}_{\mathfrak{L}M}$ symplectic generator in a m-scheme basis can be written as

$$\begin{aligned}\langle n_f l_f j_f m_{jf}|A^{(20)}_{\mathfrak{L}M}|n_i l_i j_i m_{ji}\rangle &= \frac{A-1}{\sqrt{2}A}\delta_{n_f n_i+2}(-1)^{\phi}\\ &\times \sqrt{2\mathfrak{L}+1}\sqrt{2j_i+1}C^{j_f m_{jf}}_{j_i m_{ji}\mathfrak{L}M}\begin{Bmatrix} l_i & \frac{1}{2} & j_i\\ j_f & \mathfrak{L} & l_f\end{Bmatrix}\\ &\times \sum_{n_t l_t}\begin{Bmatrix}1 & 1 & \mathfrak{L}\\ l_i & l_f & l_t\end{Bmatrix}\langle n_f l_f||b^\dagger||n_t l_t\rangle\langle n_t l_t||b^\dagger||n_i l_i\rangle,\end{aligned}$$

where $\phi = \frac{3}{2}+\frac{\mathfrak{L}}{2}+2l_f+j_i+l_i$ and A denotes the total number of nucleons.

An additional term introduced in the symplectic raising generator (3) to remove the spurious center-of-mass motion is a two-body operator. Two body matrix elements of the $A^{(20)}_{\mathfrak{L}M}$ symplectic generator in a m-scheme basis can be written as

$$\begin{aligned}&\langle n_1' l_1' j_1' m_{j1}'; n_2' l_2' j_2' m_{j2}'|A^{(20)}_{\mathfrak{L}M}|n_1 l_1 j_1 m_{j1}; n_2 l_2 j_2 m_{j2}\rangle\\ &= \frac{\sqrt{2}}{A}(-1)^{\chi}\langle n_1' l_1'\|b^\dagger\|n_1 l_1\rangle\langle n_2' l_2'\|b^\dagger\|n_2 l_2\rangle\\ &\times\sqrt{(2j_1+1)(2j_2+1)}\begin{Bmatrix} l_1 & \frac{1}{2} & j_1\\ j_1' & 1 & l_1'\end{Bmatrix}\begin{Bmatrix} l_2 & \frac{1}{2} & j_2\\ j_2' & 1 & l_2'\end{Bmatrix}\\ &\times\sum_{\alpha,\beta=0,\pm1}C^{j_1' m_{j1}'}_{j_1 m_{j1} 1\alpha}C^{\mathfrak{L}M}_{1\alpha 1\beta}C^{j_2' m_{j2}'}_{j_2 m_{j2} 1\beta}\end{aligned}$$

with $\chi = j_1 + l_1' - j_2 - l_2' + \mathfrak{L}/2$.

APPENDIX B: MATRIX ELEMENTS OF THE ELECTRIC QUADRUPOLE MOMENT OPERATOR $\hat{Q}_{2\mu}$

The $\hat{Q}_{2\mu}$ electric quadrupole moment operator is an element of the $\mathfrak{sp}(3, \mathbb{R}) \supset \mathfrak{su}(3)$ algebra and generates $0\hbar\Omega$ and $2\hbar\Omega$ quadrupole transitions. It is a spherical tensor with orbital angular momentum 2 and projection μ and can be expressed as

$$Q_{2\mu} = \sqrt{6}[r_1 \times r_1]_{2\mu},$$

where

$$r_{1\mu} = \frac{1}{\sqrt{2}}(b^\dagger_{1\mu} + b_{1\mu})$$

is the proton coordinate operator in spherical coordinates. Matrix elements of the electric quadrupole moment operator

in a m-scheme basis can be therefore written as

$$\begin{aligned}&\langle n_f l_f j_f m_{jf}|Q_{2\mu}|n_i l_i j_i m_{ji}\rangle \\ &= \sqrt{\frac{15}{2}}(-1)^{\varphi}\sqrt{(2j_i+1)}C^{j_f m_{jf}}_{j_i m_{ji} 2\mu}\begin{Bmatrix} l_i & \frac{1}{2} & j_i \\ j_f & 2 & l_f \end{Bmatrix} \\ &\times \sum_{n_t l_t}\begin{Bmatrix} 1 & 1 & 2 \\ l_i & l_f & l_t \end{Bmatrix}\langle n_f l_f\|(b_1^{\dagger}+b_1)\|n_t l_t\rangle \\ &\times \langle n_t l_t\|(b_1^{\dagger}+b_1)\|n_i l_i\rangle,\end{aligned}$$

where $\varphi = \frac{1}{2} + l_i + j_i$. These matrix elements are used to determine $B(E2: J_f \to J_i)$ transition rates, which in e^2 fm^4 units are calculated as follows,

$$B(E2) = \frac{1}{2J_i+1}\frac{5}{16\pi}\left(\frac{\hbar}{m\omega}\right)^2 |\langle J_f\|Q_2\|J_i|^2\rangle.$$

The reduced matrix elements of the HO ladder operators, $b^{\dagger}$ and b, given in a phase convention with the radial part of the HO wave function positive at infinity have the form,

$$\begin{aligned}\langle n_f l_f\|b_1^{\dagger}\|n_i l_i\rangle &= (-\sqrt{l_i}\sqrt{n_i - l_i + 2}\delta_{l_f,l_i-1} \\ &\quad + \sqrt{l_i+1}\sqrt{n_i + l_i + 3}\delta_{l_f,l_i+1})\delta_{n_f,n_{i+1}} \\ \langle n_f l_f\|b_1\|n_i l_i\rangle &= (-\sqrt{l_i}\sqrt{n_i + l_i + 1}\delta_{l_f,l_i-1} \\ &\quad + \sqrt{l_i+1}\sqrt{n_i - l_i}\delta_{l_f,l_i+1})\delta_{n_f,n_{i-1}}.\end{aligned}$$

[1] P. Navrátil, J. P. Vary, and B. R. Barrett, Phys. Rev. Lett. **84**, 5728 (2000); Phys. Rev. C **62**, 054311 (2000).
[2] P. Navrátil and B. R. Barrett, Phys. Rev. C **57**, 562 (1998); **59**, 1906 (1999); P. Navrátil, G. P. Kamuntavičius, and B. R. Barrett, *ibid*. **61**, 044001 (2000).
[3] P. Navrátil and W. E. Ormand, Phys. Rev. C **68**, 034305 (2003).
[4] A. M. Shirokov, A. I. Mazur, S. A. Zaytsev, J. P. Vary, and T. A. Weber, Phys. Rev. C **70**, 044005 (2004); A. M. Shirokov, J. P. Vary, A. I. Mazur, S. A. Zaytsev, and T. A. Weber, Phys. Lett. **B621**, 96 (2005); A. M. Shirokov, J. P. Vary, A. I. Mazur, and T. A. Weber, *ibid*. **B644**, 33 (2007).
[5] R. Machleidt, F. Sammarruca, and Y. Song, Phys. Rev. C **53**, R1483 (1996); R. Machleidt, *ibid*. **63**, 024001 (2001).
[6] D. R. Entem and R. Machleidt, Phys. Rev. C **68**, 041001(R) (2003).
[7] T. Dytrych, K. D. Sviratcheva, C. Bahri, J. P. Draayer, and J. P. Vary, Phys. Rev. Lett. **98**, 162503 (2007).
[8] G. Rosensteel and D. J. Rowe, Phys. Rev. Lett. **38**, 10 (1977).
[9] D. J. Rowe, Rep. Prog. Phys. **48**, 1419 (1985).
[10] G. Rosensteel and D. J. Rowe, Ann. Phys. (NY) **126**, 343 (1980).
[11] J. P. Draayer, K. J. Weeks, and G. Rosensteel, Nucl. Phys. **A413**, 215 (1984).
[12] J. Escher and A. Leviatan, Phys. Rev. C **65**, 054309 (2002).
[13] F. Arickx, J. Broeckhove, and E. Deumens, Nucl. Phys. **A377**, 121 (1982).
[14] S. S. Avancini and E. J. V. de Passos, J. Phys. G **19**, 125 (1993).
[15] T. Dytrych, K. D. Sviratcheva, C. Bahri, J. P. Draayer, and J. P. Vary, to be submitted to Phys. Rev. C.
[16] K. T. Hecht and D. Braunschweig, Nucl. Phys. **A295**, 34 (1978); Y. Suzuki, Nucl. Phys. **A448**, 395 (1986).
[17] G. Rosensteel, Astrophys. J. **416**, 291 (1993).
[18] J. P. Vary, "The Many-Fermion-Dynamics Shell-Model Code," Iowa State University, 1992 (unpublished); J. P. Vary and D. C. Zheng, *ibid*. 1994 (unpublished).
[19] Y. Funaki, A. Tohsaki, H. Horiuchi, P. Schuck, and G. Röpke, Phys. Rev. C **67**, R051306 (2003).
[20] A. P. Zuker, B. Buck, and J. B. McGrory, Phys. Rev. Lett. **21**, 39 (1968).
[21] P. J. Ellis and T. Engeland, Nucl. Phys. **A144**, 161 (1970).
[22] T. Engeland and P. J. Ellis, Nucl. Phys. **A181**, 368 (1972).
[23] W. C. Haxton and C. Johnson, Phys. Rev. Lett. **65**, 1325 (1990).
[24] E. K. Warburton, B. A. Brown, and D. J. Millener, Phys. Lett. **B293**, 7 (1992).
[25] D. J. Millener, A. C. Hayes, and D. Strottman, Phys. Rev. C **45**, 473 (1992).